SELF-HEALING AND IONIC INTERACTIONS: A LOOK INTO THERMAL PROPERTIES OF SEQUENCE-SPECIFIC IONIC NETWORKS AND THE SYNTHESIS OF SPIROPYRAN MONOMERS FOR TRIGGERD IONIC NETWORKS

BY

ANDERSON COATES

THESIS

Submitted in partial fulfillment of the requirements
for the degree of Master of Science in Chemistry
in the Graduate College of the
University of Illinois at Urbana-Champaign, 2016

Urbana, Illinois

Adviser:

Professor Jeffrey S. Moore

Abstract

Self-healing is essential in future materials for extending lifetime beyond normal limits and lowering operational cost over extended use. Of the structural approaches to self-healing, an intrinsic system provides capability for multiple healing cycles based on reversible healing processes. Of these processes, ionic interactions provide the basis for reversible self-healing systems from organic ion associations and metal-ligand coordination.

In my investigation of organic ion associations, I probed the effects of oligomer sequence on the thermal stability of guanidium-phosphate associations in DNA ionic networks. Each network contained a different five monomer sequence of DNA using two monomers crosslinked by bis(guanidinium) dications. Measuring the thermal properties by differential scanning calorimetry for all 32 ionic network sequences and comparing their properties lead to structural trends that increase overall ionic network stability indicated by a higher degradation temperature. Substituting in the more flexible monomer at one chain end lead to an increase in degradation temperature in 13 pairs of sequences. However, substitution at the other oligomer chain end did not produce a similar temperature increase. This is due to the increased flexibility of one chain end providing more stabilizing interactions during the evaporation phase of sample preparation. Due to the sequence-specific and monodisperse nature of automated DNA synthesis, a small change in the oligomer structure produces measurable effects on thermal properties. Understanding the contributions of each monomer leads to total control of a material's properties for optimal material design.

Investigation of metal-ligand coordination in self-healing began with a collaboration focused on synthesizing spiropyran polymers that reversibly form ionic crosslinks on stimulation by force or UV light in a self-strengthening process. Reversible crosslinking in a stimuli responsive material provides strengthening and relaxation in cycles that counteracts fatigue to prolong material lifetime. Under stimulus, spiropyran opens to zwitterionic merocyanine which coordinates to metal ions as a ligand. Modifying spiropyran with coordinating sidechains controls the ratio of spiropyran molecules to metal ions such that two or more spiropyran molecules coordinate to a single ion. In polymers containing modified spiropyran, this multiple spiropyran to ion coordination allows the formation of ionic crosslinks that trigger on force or UV light and return to the original state on removing stimuli. My collaborators and I synthesized spiropyran and spirooxazine monomers with coordinating sidechains to analyze the ion coordination stoichiometry to probe candidates for triggered and reversible ionic crosslinking. Spiropyran with a para-nitro group stabilized merocyanine such that consistent red color was observed in the solid state polymer and solution. This drove efforts toward developing new synthesis routes with less potent electron withdrawing groups. We synthesized a naphthalene spirooxazine that showed photochromism at

low temperature, and we have a promising start on synthesizing spiropyran monomers with less powerful electron withdrawing groups. Developing these syntheses of other electron withdrawing groups in spiropyran and spirooxazine will lead to candidates for triggered ionic crosslinking for reversible self-strengthening systems.

Acknowledgments

My journey in graduate school would not be possible without my adviser, Professor Jeffrey S. Moore, who gave me a chance when I needed it most. Additionally, he provided constant opportunities for success and collaboration, and his feedback was always constructive and helpful. I am thankful for all the other graduate students, post-docs, and undergraduate students in the Moore group who made working in the lab as much fun as graduate school can be.

The work represented here is with the aid of and in collaboration with other graduate students at the University of Illinois at Urbana-Champaign. For chapter 1, Ke Yang of the Moore group was instrumental in helping start this project. His guidance was especially helpful with the guanidinium synthesis and DSC analysis. Benjamin Brandsen of Professor Scott Silverman's group ran the DNA synthesizer for the oligomers. The work in chapter 2 was in collaboration with Eric Epstein and Shuqi Lai from the group of Professor Paul Braun. Eric collected and analyzed the UV-Vis data and completed the spiropyran and spirooxazine syntheses.

Table of Contents

Introduction

Self-healing is a fundamental property for future materials to overcome the natural wear that leads to failure. With a productive response to its environment, a self-healing material survives damaging events that reduce material safety and lifetime. With a longer lifetime, materials become more cost effective during prolonged use.

Self-healing follows three structural strategies: capsule, vascular, and intrinsic.[1] Both capsule and vascular rely on delivering healing agents to a damaged site to for the healing reaction. However, the amount of healing agent sequestered in the material limits the amount of damage these systems can repair. To surpass this limit, intrinsic healing uses latent structural functionality in the matrix that activates a healing response on damaging stimuli. These healing responses are often based on reversible bonds which allows multiple healing cycles to survive multiple damaging events over a longer time.

Studying a self-healing system based on ionic interactions provides an opportunity to utilize the reversible nature of organic ion associations and metal-ligand coordination. These systems are called ionic networks where ionic interactions provide crosslinking that forms a network. Presented here are my efforts in starting two project in ion-based self-healing systems. To probe the nature of organic ion associations, my first project focused on the effect of oligomer sequence on the thermal stability of guanidinium-phosphate interactions in sequence specific DNA ionic networks. To investigate metal-ligand coordination, my second project is a collaborative effort to create a reversible self-strengthening system based on triggered ionic crosslinking in spiropyran polymers.

Chapter 1: The Effect of Oligonucleotide Sequence on the Thermal Properties of Crosslinking Ionic Networks

1.1 Introduction

DNA oligomers have potential applications as high density information storage devices, nanomaterials, and biomedicine.[2,3] However, the thermal stability of DNA oligonucleotides varies depending on sequence.[4] Similar to metal ions crosslinking polyphosphates, multi-valent cations increase thermal stability through forming ionic crosslinks between chains via the backbone phosphate anions.[5] This gain in thermal stability from crosslinking further increases through finding sequences that favor strong interactions. To investigate the thermal stability gained from crosslinking ions, solid-phase DNA synthesizers produce oligomers with specific sequences from a diverse range of monomers.[3,6] Combining sequence-specificity and monomer diversity allows for precise structure-property studies to probe the extent that thermal stability can increase from monomer placement in the oligomer sequence. Knowing structure-property trends allows for the design of precision materials where each monomer has a known contribution tailored toward the desired property or function.

From examples in nature, guanidinium interacts well with the backbone phosphate groups providing handles for crosslinking ionic interactions that improve thermal stability. From protein-DNA cocrystal structures, phosphate associates most often with the guanidinium group of arginine.[7] These associations are stabilized through charge interactions and hydrogen bonding. With both interactions, guanidinium produces stronger associations than metal cations alone. Greater stabilization in each ionic interaction results in a more thermally stable material. While guanidinium has been used with polymer-plasmid interactions[8], the thermal stability of guanidinium ionic interactions has not been shown in materials.

The effect of guanidinium stabilization depends on DNA oligomer sequence. Each monomer contributes to the overall thermal stability such that discovering structural or sequence trends in this first series dictates design of subsequent series of oligomers. Each subsequent series elucidates new trends ultimately leading to the most optimized sequence. With the absolute sequence control that a DNA synthesizer provides, this synthesis-testing-refinement cycle has not been reported for material property optimization.

This work is the first systematic series of ionic networks made from five monomer (5-mer) oligomers containing deoxyguanosine (**G**) and hexaethylene glycol (**s**) (Chart 1). Both monomers

produced monodisperse, sequence-specific oligomers on a DNA synthesizer.[6] Additionally, (**G**) provides multiple sites for association which allows interactions beyond ionic crosslinking for additional thermal stability.[9] There are 32 possible combinations of (**G**) and (**s**) in a 5-mer. Each combination was synthesized and crosslinked into ionic networks using a bis(guanidinium) isophthalamide dication. For each network, the heat flow was measured by differential scanning calorimetry (DSC). Through relating the DSC curves to thermal stability, sequence trends were found that increased ionic network strength.

1.2 Experiment Design

An automated DNA synthesizer made the 32 possible 5-mers following standard procedures with extended monomer coupling time. The bis(guanidinium) dication (**1**) crosslinker was synthesized in one step from dimethyl isophthalate and guanidine hydrochloride. The oligomer and dication were run through cation and anion exchange columns respectively. Post-ion-exchange oligomer and dication solutions in methanol were combined to produce ionic network samples. For DSC thermal analysis, ionic network samples were added to pans and concentrated under vacuum.

The names of oligomer sequence positions are defined following the same naming convention as the deoxyribose ring in DNA (Chart 1). The 5′ to 3′ directionality refers to carbons bonded to phosphate in the deoxyribose ring. The (**s**) monomer maintains directionality by labeling phosphate at the 3′ end by definition. Sequences are written in the 5′ to 3′ direction such that the 3′ monomers end with phosphate.

1.3 Identifying Ionic Network Degradation

During DSC analysis, all ionic network samples experienced a large thermal event just above 100 °C corresponding to degradation of the network. On the second heating cycle, DSC curve events were not consistent with the first cycle which signals sample degradation. This was consistent across multiple runs for each ionic network. Thermogravimetric analysis (TGA) provided evidence for degradation (Figure 1). After evaporation of residual methanol in the 25-50 °C region, the next mass loss falls within the 115-130 °C region. This temperature range corresponds the degradation DSC peak that occurs for all 32 ionic networks. Since this degradation event causes mass loss over a broad temperature range for each network in this study, this DSC event is caused by gradual network degradation.

1.4 Sequence Effects in the Degradation Peak

Comparing the degradation peak common to all of the ionic network samples, I found sequence effects based on temperature differences between sequence pairs. Figure 2 shows the differences between final and initial temperature for when (**s**) replaces (**G**) at the terminal 3′ position. The average onset

temperature increases in 13 sequence pairs by 4-17 °C. Two pairs have deviations intersecting zero temperature difference, and the remaining case decreases.

As a possible rationalization, this temperature increase is due to the increase in flexibility from substituting (**s**) in the place of (**G**). The internal 3′ phosphate is less hindered by substituting the rigid ribose ring for a linear 18-atom chain. From the increased flexibility, the phosphate has a broader range of motion and more chances to find optimal associations while in the solution phase. With more optimal associations, the ionic network becomes more thermally stable on evaporation.

This validity of this explanation depends on the ionic interaction reversibility. Based on guanidinium-carboxylate association in 10 vol% water in methanol,[10] guanidinium-phosphate interactions may have varying association constants at room temperature depending on phosphate group proximity. As solvent evaporates at a constant rate, low volume restricts chain motion. In this low volume state, the flexible (**s**) phosphates find optimal interactions through rapid association/dissociation interactions. Through a large amount of association/dissociation, flexible phosphate groups form the most optimal interactions in the timeframe for solvent evaporation. When the solution reaches the precipitation point, the ionic networks with flexible phosphates contain the most stable associations possible. Through this reasoning, easily reversible binding allows flexibility to have the greatest effect.

The less reversible case follows a kinetic argument that minimizes the terminal 3′ (**s**) flexibility effect. Phosphate interactions take more time to dissociate compared to the easily reversible case. With a constant solvent evaporation rate, phosphates make fewer association/dissociation interactions before precipitation. Fewer interactions mean that (**s**) cannot reach the same optimal associations as in the easily reversible case. Without the most optimal interactions, (**s**) and (**G**) make associations with similar stability causing the flexibility effect to disappear.

Searching for other structural/sequence relationships, I examined the degradation peak onset temperatures for sequences with one monomer substitution, G4/s1 and G1/s4 (Figure 3). The GGGGG sequence onset temperature is higher than those for most G4/s1 sequences due to guanine base self-interactions which further increases the network thermal stability. Guanine self-associates in a variety of different structures using both Watson-Crick and Hoogstein faces (Chart 2).[9] The G-duplex and G-ribbon are the likely self-association patterns for this system because they involve the fewest guanine bases. Sequences rich in (**G**) use these secondary structures to form more stable interactions and additional crosslinks. Placing (**s**) into the sequence interrupts guanine self-interactions decreasing the onset temperatures. However, since GGGGs has one of the highest temperatures, an optimal mix of (**G**) and (**s**)

exists that gives the flexibility to facilitate both guanine interactions and phosphate associations simultaneously.

Observing the flexible sequences containing four (**s**), the G1/s4 sequences have onset temperatures on par with sssss and GGGGG (Figure 3). When (**G**) is at the terminal 5′ position, onset temperature increases compared to sssss due to flexibility at the chain end. For internal (**G**), this flexibility effect is dampened by charge repulsion between backbone phosphate groups hindering chain motion. However, the sssGs sequence gives the highest temperature in the series. This high temperature is the result of both terminal 3′ (**s**) flexibility and additional guanine associations at this position. Because the same temperature increase does not occur for sGsss, the position of (**G**) in the sequence affects the strength of guanine associations.

For comparison to the terminal 3′ (**s**) effect, substitution at the terminal 5′ position has no clear sequence effect (Figure 4). For 8 sequence pairs, there is no visible effect due to the large margin of error. However, terminal 5′ substitutions in GsssG and GsGss go from a positive to negative temperature difference as the (**G**) monomers move closer in the sequence (red bars, Figure 4). The effect is highest for sequences with GsG at the chain end suggesting that this sequence fragment strengthens guanine self-associations. Stronger guanine associations are the result of more stable G-duplex or G-ribbon structures. A GsG fragment provides the flexibility to form more stable associations. The GsG effect is the reason for the temperature decrease of the ssGsG-ssGss comparison in Figure 2.

1.5 Events at Lower Temperatures on the DSC Curve

For each ionic network, the first heating cycle in the DSC curves showed other peaks at temperatures lower than the degradation peak temperature (Figure 5). However, when using the same analysis as the degradation peak data, the lower temperature peaks did not provide any significant structure or sequence effects. All analyses were similar to Figure 4 where the temperature differences were above and below zero with no clear trend. At these lower temperatures, effects from the oligomer chain interactions and ion dissociation occur.[11] Sequences effects at lower temperature may be visible with less complex systems that minimize the amount of secondary interactions.

1.6 Conclusion

This study demonstrates the effects that single monomer substitutions make on thermal properties of DNA oligomer ionic networks. Substitutions at chain ends produce the greatest thermal stability through increasing phosphate flexibility or facilitating guanine associations as evidenced by increasing DSC peak-onset temperatures. From this study, the structure trends allow design of more thermally stable

DNA materials. These trends provide the beginning of a quantitative structure-activity relationship study similar to examples from catalytic organic reactions.[12] Understanding these relationships allows property prediction and specifically designed materials with exactly the right properties for their application.

1.7 Charts, Figures, and Tables

a

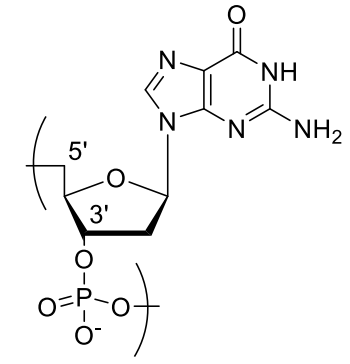

Deoxyguanosine (**G**)

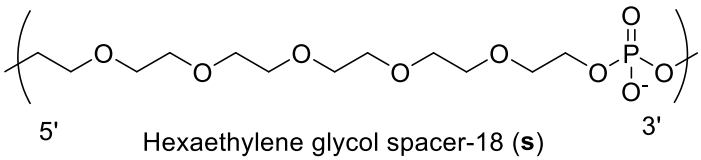

Hexaethylene glycol spacer-18 (**s**)

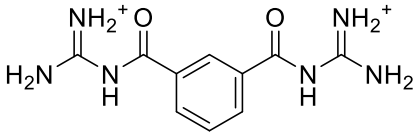

1

Bis(guanidinium) isophthalamide (dication)

b

HO—terminal 5' - internal 5' - center - internal 3' - terminal 3'—OH

5'-G-G-s-s-s-3' = GGsss, a G2/s3 sequence

c

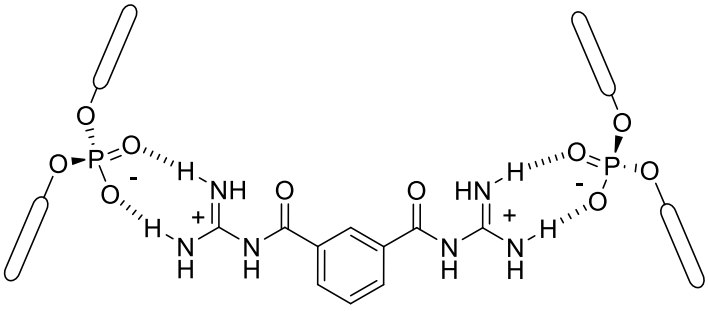

Guanidinium-Phosphate association

Chart 1. The monomers and the dication crosslinker used in this study (a), the definitions for oligomer sequence positions (b), and a possible crosslinking guanidinium-phosphate association geometry (c).

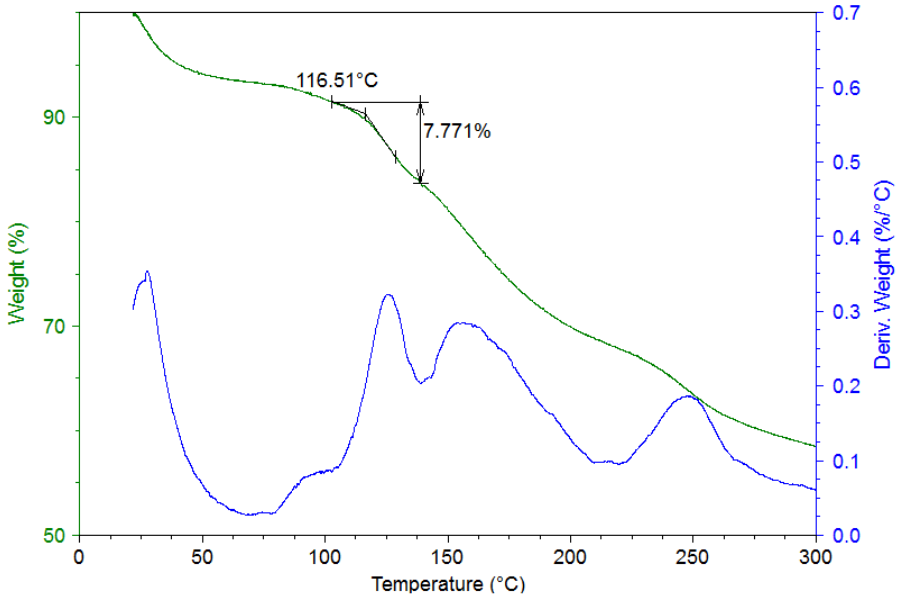

Figure 1. TGA curve of GsGsG (green, top) and its first derivative with respect to temperature (blue, bottom) at an 8 °C/min heating rate under N_2 atmosphere. Rapid mass loss occurs in the 115-130 °C region corresponding to the DSC peak onset in that temperature range.

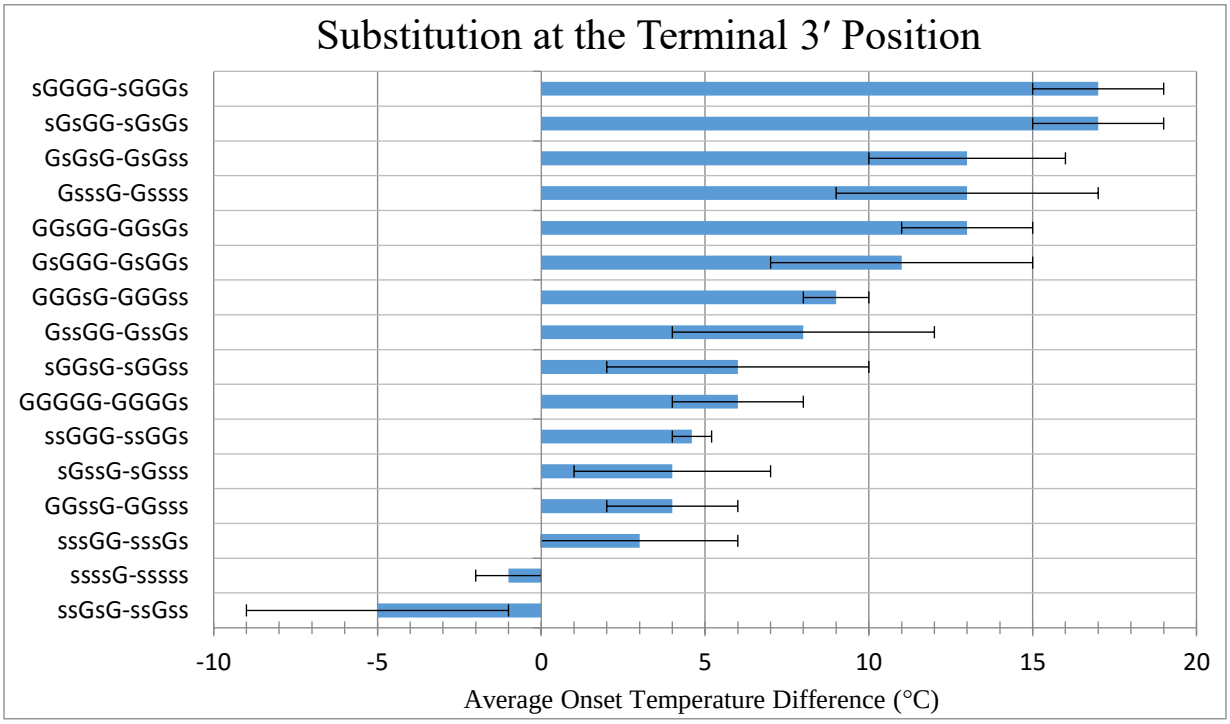

Figure 2. Onset temperature difference for ionic network sequences after substituting the monomer at the terminal 3′ position. Sequence pairs are listed "before-after" substitution. In most sequence pairs, onset temperature increases after substitution.

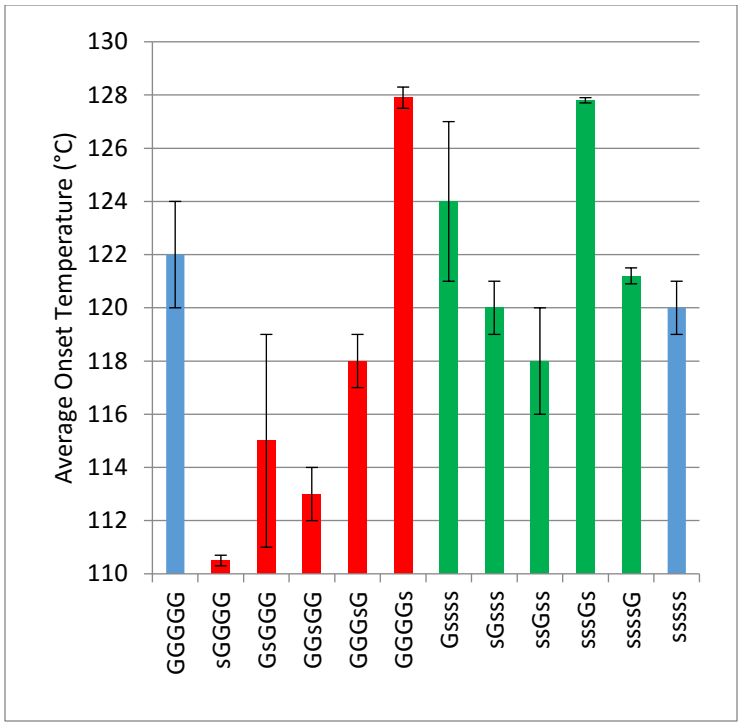

Figure 3. Comparing average peak onset temperatures between sequences with one substitution. The G4/s1 sequences (red) average lower than the G1/s4 (green) and identical monomer sequences GGGGG and sssss (blue).

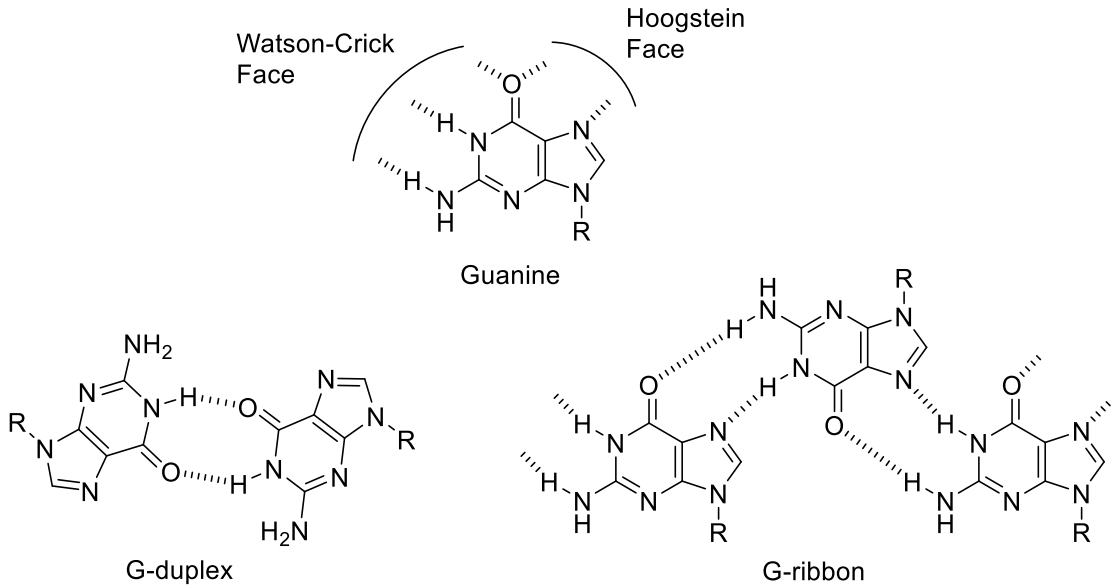

Chart 2. Guanine hydrogen bonding sites and possible patterns of self-association responsible for higher stability of (G)-rich sequences.

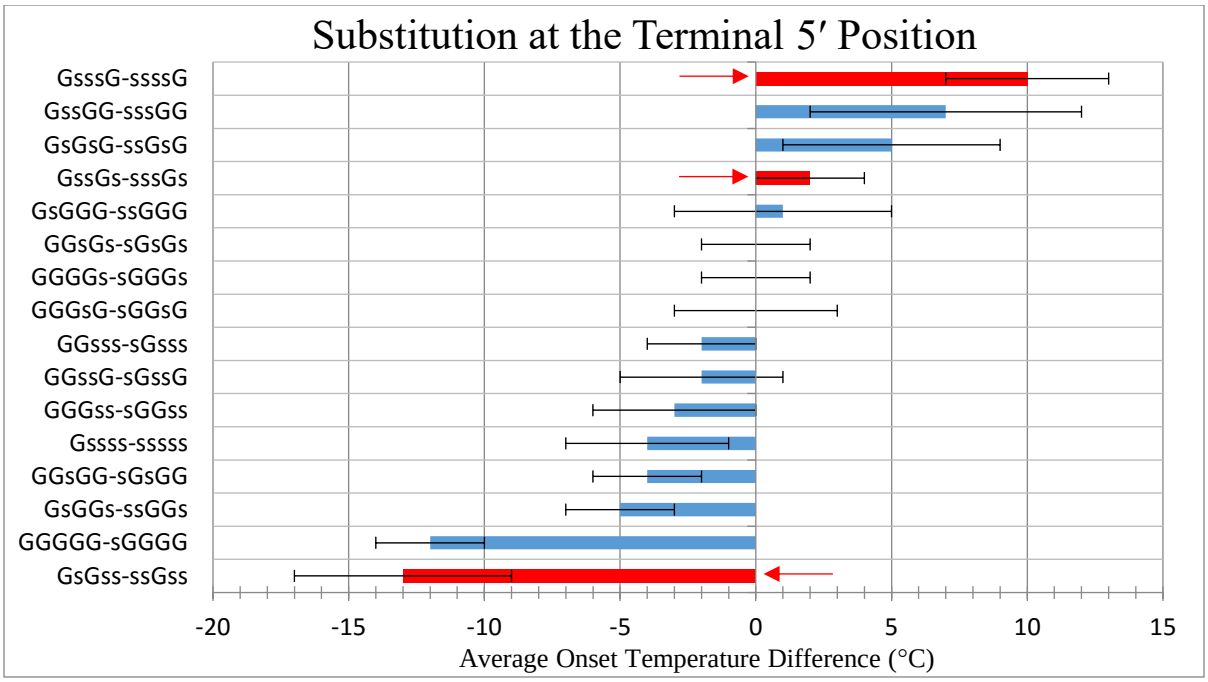

Figure 4. Onset temperature difference for ionic network sequences after substituting the terminal 5′ monomer. Sequence pairs are listed "before-after" substitution. The sequence pairs in red (arrows) suggest (**G**) in close proximity have a stabilizing effect reaching a maximum for a GsG sequence near the chain end.

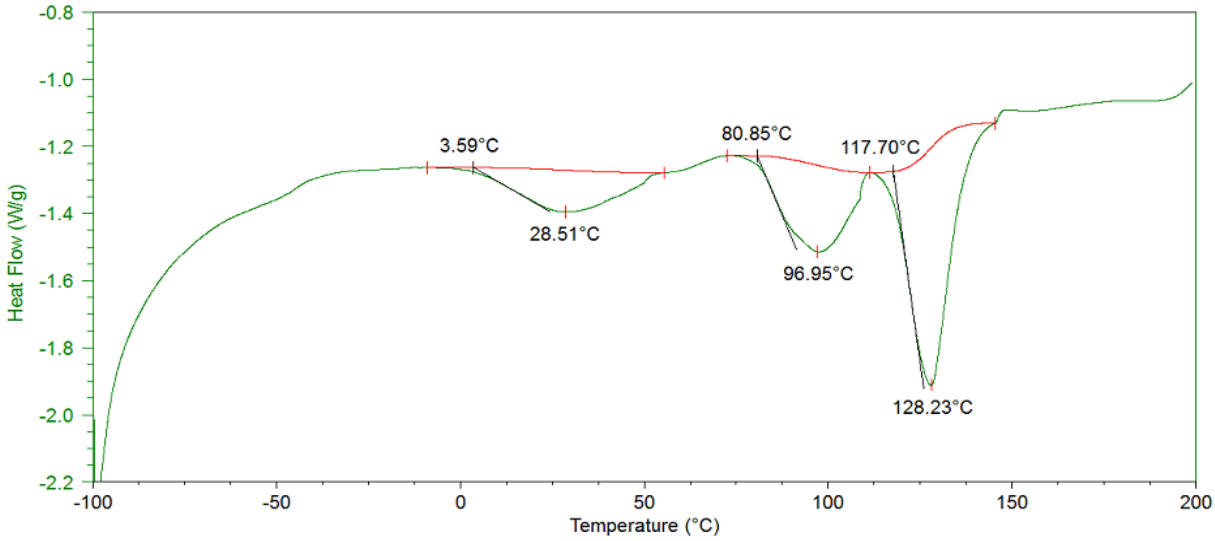

Figure 5. A first heating cycle DSC curve for GsGsG heating at 8 °C/min. The peaks correspond to oligomer chain effects, ion dissociation, and network degradation with increasing temperature. The peak onset temperatures are labeled above the curve, and peak minimum temperatures are below the curve.

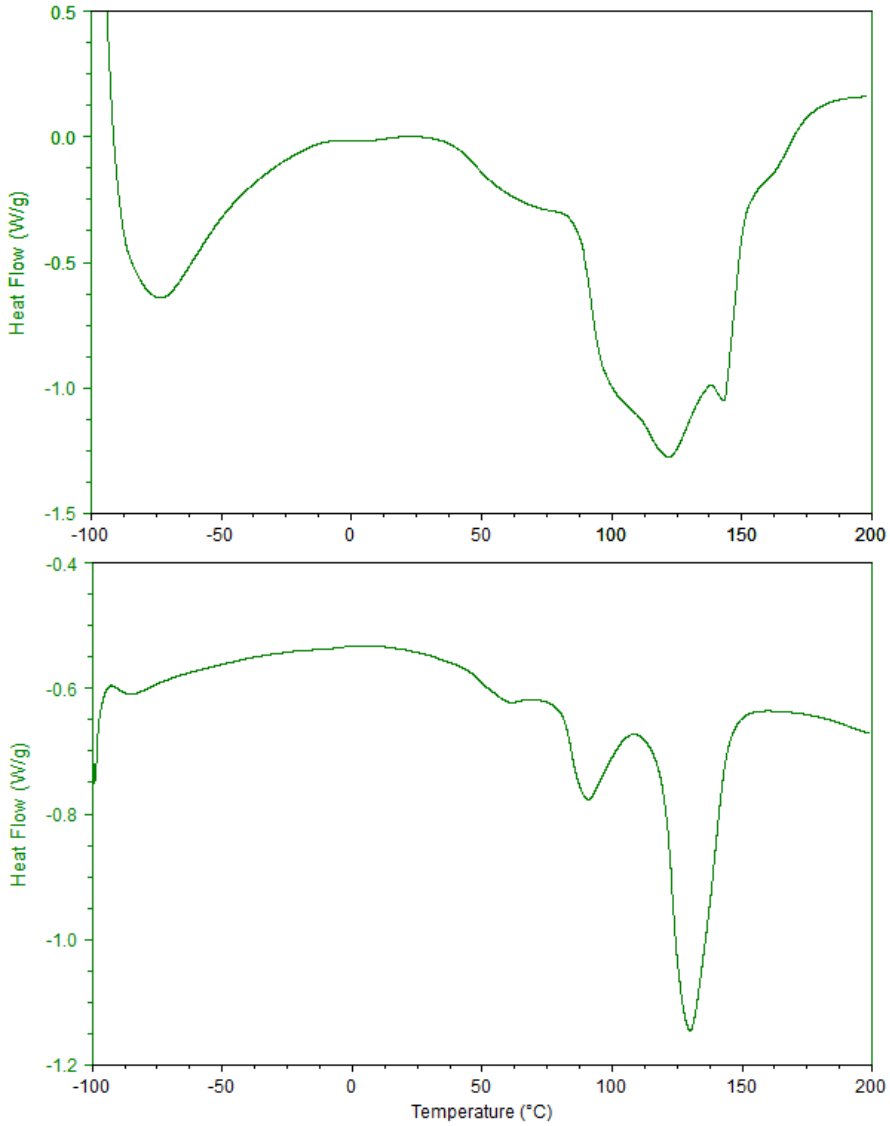

Figure 6. Comparing the DSC curves for two different runs of sGsGG. The top curve was prepared by scraping and heated at 15 °C/min, and the bottom by addition/evaporation at 8°C/min.

G5 & G4/s1	Average peak-onset Temperature (°C)	G3/s2	Average peak-onset Temperature (°C)	G2/s3	Average peak-onset Temperature (°C)	G1/s4 & s5	Average peak-onset Temperature (°C)
GGGGG	122 ± 2	ssGGG	116.0 ± 0.6	sssGG	125 ± 3	Gssss	124 ± 3
sGGGG	110.5 ± 0.2	sGsGG	109 ± 2	ssGsG	123 ± 4	sGsss	120 ± 1
GsGGG	115 ± 4	sGGsG	118 ± 3	ssGGs	120.6 ± 0.1	ssGss	118 ± 2
GGsGG	113 ± 1	sGGGs	128 ± 2	sGssG	116 ± 3	sssGs	127.8 ± 0.1
GGGsG	118 ± 1	GssGG	118 ± 4	sGsGs	126.4 ± 0.5	ssssG	121.2 ± 0.3
GGGGs	127.9 ± 0.4	GsGsG	117.8 ± 0.7	sGGss	124 ± 3	sssss	120 ± 1
		GsGGs	126 ± 2	GsssG	111 ± 3		
		GGssG	118 ± 1	GssGs	126 ± 2		
		GGsGs	126 ± 2	GsGss	131 ± 3		
		GGGss	127 ± 1	GGsss	122 ± 2		

Table 1. The average degradation peak onset temperature for the ionic networks listed by oligomer sequence. Groups are arranged by the number of (**G**). Comparing these data produced the observed sequence effects.

1.8 Experimental and Supporting Information

All reagents purchased commercially and used without additional purification. High Load Glen UnySupport and all standard reagents for the ABI 394 DNA synthesizer were purchased from Glen Research. The DMT-hexaethylene glycol spacer-18 phosphoramidite was purchased from Link Technologies, Ltd. in 250 mg quantites and diluted to 0.075 M with anhydrous acetonitrile before use. Ammonium hydroxide, 30% solution, was purchased from J.T. Baker, and methanol was from Macron. Diemthyl isophthalate, sodium hydride (60% dispersion in mineral oil), guanidine hydrochloride, and Dowex 50WX2 Hydrogen form (200-400 mesh) strong acid ion exchange resin were purchased from Sigma Aldrich. Dimethylformamide was purchased from Omnisolv. Dowex Monosphere 550A UPW strong base ion exchange resin was purchased from Supelco.

Oligomer Synthesis:

Oligomers were synthesized with 40 mg solid support following standard DNA synthesis procedures with extended 5 min coupling time. Oligomers were deprotected and cleaved from solid support with ammonium hydroxide, 30% solution; incubating at 55 °C for 14 h. Ammonium hydroxide solution was evaporated overnight in speed vac concentrator. Oligomers were dissolved in methanol, and residual solid support was filtered off. Filtrate yielded isolated oligomer having a clear film appearance. Oligomer was weighed resulting in approximately 2 mg for each sequence.

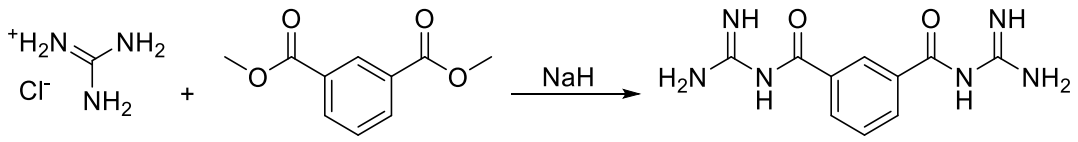

1

(1) Bis(guanidinium) isophthalamide/N1,N3-dicarbamimidoylisophthalamide:

Bis(guanidinium) isophthalamide (**1**) was synthesized following similar literature method.[13] To a solution of guanidine hydrochloride (15.7 mmol) in DMF (17 mL) at 0 °C, NaH (15.7 mmol) was added portionwise. The mixture was stirred at room temperature for 2.5 h. To the mixture, a solution of dimethyl isophthalate (3.9 mmol) in DMF (21 mL) was added dropwise. The mixture was stirred at 70 °C for 17h. After cooling, the reaction mixture was concentrated *in vacuo*. The remaining solids were collected by filtration, washed with DMF for 30 min, and dried *in vacuo* at 50 °C. 62% yield; ^{1}H NMR (DMSO-d_6) δ: 8.45 (s, 2H), 7.60 (br s, 10H); MS (HR ESI): m/z = 249.1102 (M^++H), calc. 249.1100 $C_{10}H_{13}N_6O_2$

Ionic Network Formation:

Oligomer samples were run through a strong acid ion exchange column, and dication samples were run through a strong base ion exchange column before combination. An approximate 10-fold amount of each resin was used, calculated from the milliequivalents per mL of wet resin. Amounts of resin were measured in a graduated cylinder filled with methanol allowing 30 min for resin wetting. Wet resin was added to the column and washed with methanol until eluate was clear. Samples of dication were weighed and dissolved in 5 mL of methanol before ion exchange. Oligomer samples were dissolved in 0.5 mL methanol and often required vortex mixing to dissolve. Sample solutions were added to resin in the column via syringe. The syringe was washed with methanol, and methanol was added to wash the column. Approximately 3-4 column-volumes of methanol were used to flush the resin of residual sample. The column was continually flushed with argon, and eluate was collected in a vial under argon.

Post-ion-exchange solutions of oligomer and dication were mixed to synthesize the ionic network. Molarity of the post ion-exchange dication solution was calculated by measuring the methanol solvent's mass and then converting to volume. The previously measured mass of dication was converted to moles and was divided by the methanol volume to give the molarity. For charge neutralization between dication and oligomer, a 10:2 mole ratio solution of dication to oligomer was made by adding the appropriate amount of post-ion-exchange dictation solution to the post-ion-exchange oligomer solution. The ionic network solution was evaporated slowly to dryness. High vacuum over 16 h was used to remove remaining methanol. The ionic network solid was white and adhered to vial walls.

DSC and TGA Analyses:

Ionic network samples were analyzed by differential scanning calorimetry (DSC) on a TA Instruments Q20 differential scanning calorimeter with Tzero aluminum pans. Due to low sample masses, transfer of solid ionic network from vial to the Tzero pan was impossible for all samples. Ionic network samples were dissolved in methanol, and the solution was added to Tzero pans for evaporation. Successive rounds of solution addition and evaporation were performed until approximately 0.2 mg solid was in the pan. The pans and lids were placed on high vacuum until dry, approximately 24 h. The DSC protocol followed a heat/cool/heat cycle with the following parameters: -100 °C to 200 °C at 8 °C/min, 200 °C to -100 °C at 15 °C/min, and -100 °C to 150 °C at 15 °C/min. The heating rates and temperatures were chosen based on time constraints from number of samples for analysis and method run time. The slower first heating rate was chosen because the analyzed events on the DSC curve appear in this segment.

Events on the DSC curve were inconsistent when comparing multiple runs of one sample due to network degradation after the first heating cycle. To find repeatable events, I averaged the temperatures occurring near a similar value for multiple runs of a sample solution. This averaging requires consistent sample preparation procedures. Early in the data collection process, samples with larger quantity were scraped into Tzero pans rather than through addition/evaporation of the stock solution. Additionally, a 15 °C/min heating rate was used to save time on the high number of samples. The faster heating rate and differing sample preparation lead to uneven sample heating causing lower resolution DSC curves (Figure 6). With a slowing the heating rate, resolution dramatically improved, and the addition/evaporation method could be applied to samples that were resistant to scraping.

Thermogravimetric analysis (TGA) was performed on a TA Instruments Q50 analyzer with a platinum crucible. Crucible was tared on the instrument under nitrogen atmosphere. Ionic network solution was added to the crucible and evaporated until approximately 0.2 mg solid was transferred. Sample and crucible were dried *in vacuo* for 3 h before measurement. Sample was heated at a rate of 8 °C/min under nitrogen atmosphere. Mass loss was recorded over a 25 °C to 1000 °C temperature range.

1.9 References

1. Blaiszik B.J. et al. *Annu. Rev. Mater. Res.*, **2010**, *40*, 179-211.
2. Amin, R. et al. *Nanoscale Res. Lett.*, **2013**, *8*:119.; Luo, D. et al. *Acc. Chem. Res.*, **2014**, *47*, 1902-1911.
3. Lutz, J. F.; Badi, N. *Chem. Soc. Rev.,* **2009**, *38*, 3383-3390.
4. SantaLucia, Jr., J.; Allawi, H. T.; Seneviratne, P. A. *Biochemistry*, **1996**, *35*, 3555-3562.; Delaney, S.; Volle, C. B.; Jarem, D. A. *Biochemistry*, **2012**, *51*, 52-62.; Giancola, C. et al. *J. Am.*

Chem. Soc., **2005**, *127*, 16215-16223.; Giancola, C. et al. *Biochemistry*, **2004**, *43*, 4877-4884.; Schwalbe, H.; Lannes, L.; Halder, S.; Krishnan, Y. *ChemBioChem*, **2015**, *16*, 1647-1656.; Schwartz, F. P.; Ramprakash, J.; Lang, B. *Biopolymers*, **2008**, *89*, 969-979.

5. Bauer, H.; Hoerold, S.; Krause, W.; Sicken, M. Pulverulent Flame-Retardant Composition with Low Dust, its Use, and Process for its Preparation, and Flame-Retardant Polymeric Molding Compositions. U.S. Patent 0032958 A1, Feb. 10, 2005.
6. Sleiman, H. F.; Serpell, C. J.; Edwardson, T. G. W.; Carneiro, K. M. M. *Angew. Chem. Int. Ed.*, **2014**, *53*, 4567-4571.
7. Thornton, J. M.; Luscombe, N. M.; Laskowski, R. A. *Nucleic Acids Res.*, **2001**, *29*, 2860-2874.
8. Pun, S. H. et al. *Biomater. Sci.*, **2013**, *1*, 736-744.; Timin, A. S.; Solomonov, A. V.; Rumyantsev, E. V. *J. Polym. Res.*, **2014**, *21*, 400.
9. Sivakova, S.; Rowan, S. J. *Chem. Soc. Rev.*, **2005**, *34*, 9-21.
10. Hamilton, A. D.; Albert, J. S.; Goodman, S. *J. Am. Chem. Soc.*, **1995**, *117*, 1143-1144.
11. Basak, P. et al. *J. Phys. Chem. C*, **2014**, *118*, 159-174.; Schwarz, F. P. et al. *Biopolymers*, **2008**, *89*, 969-979.
12. Sigman, M. S.; Toste, F. D.; Milo, A.; Neel, A. J. *Science*, **2015**, *347*, 737-743.; Sigman, M. S.; Bess, E. N.; Bischoff, A. J. *Proc. Natl. Acad. Sci. U.S.A.*, **2014**, *111*, 14698-14703. Sigman, M. S.; Davies, H. M. L.; Bess, E. N.; Guptill, D. M. *Chem. Sci.*, **2015**, *6*, 3057-3062.
13. Moritomo, A. et al. *Bioorg. Med. Chem.*, **2014**, *22*, 6026-6038.

Chapter 2: Synthesis of Spiropyran and Spirooxazine Monomers for Triggered Ion Coordination in Self-Strengthening Polymers

2.1 Introduction

Under a stimulus such as force or UV light, a self-strengthening material improves bulk moduli and other properties to survive typically destructive forces.[14] This self-strengthening response increases material safety and prolongs material lifetimes by preventing failure which reduces long-term cost. An example of a self-strengthening system involves covalent bond crosslinking via mechanochemical activation of *gem*-dibromocyclopropanes.[14] Another example forms crosslinks via UV light activated radicals that polymerize latent methacylate groups.[15] In both cases, irreversible covalent crosslinks form as part of the self-strengthening process which inherently limits the number of strengthening cycles. To increase the number of cycles, materials need a strengthening mechanism that forms reversible crosslinks to allow the material returns to its original state on removing stimuli. This kind of reversible crosslinking system is possible through triggered ligands and ion coordination. Presented here are the beginning syntheses of a reversible self-strengthening system where force or UV light triggers ligand behavior in spiropyran and spirooxazine polymers to form crosslinks through metal ion coordination.

Spiropyran (SP) exists in equilibrium with its zwitterionic merocyanine (MC) form which coordinates with ions as a ligand (Scheme 1a).[16] Generally, the SP/MC equilibrium shifts to favor the colored MC in UV light, and it reverts back to a colorless or yellow SP in visible light. This generation of color in response to light is called photochromism. In polymers, force promotes this equilibrium shift in a similar reversible manner.[16] Both light and force provide triggers for MC ion coordination; however, crosslinking through ion coordination requires a 2:1 SP molecule to ion ratio (Scheme 1b). Drawing from examples in SP-ion coordination, my collaborators and I tune the electronics and steric bulk around the MC phenolate anion to favor 2:1 coordination in SP polymers. Through modifying electron withdrawing groups and coordinating sidechains, we hope to generate reversible ionic crosslinks that trigger with force or UV light then disappear on removing stimuli. Using this crosslinking mechanism, materials respond to force becoming stronger and revert back to the original state after removing force. These materials are capable of multiple cycles of strengthening and reversion and will have longer material lifetimes capable of surviving fatigue for longer than irreversible covalent systems.

Tuning the spiropyran-ion coordination ratio requires modification of the electron withdrawing groups and coordinating sidechains. Spiropyran forms from the condensation of a 2-methyleneindoline and an *o*-hydroxybenzaldehyde. We modified the R groups of both components to promote triggered 2:1 ion coordination and introduce polymerizable functional groups (Scheme 2). Groups at $R_1/R_{1'}$ and R_3

include hydroxyl moieties for polymerization. Additionally, R_3 includes a coordinating sidechain. Electron withdrawing groups at R_2 control MC concentration through stabilizing the phenolate anion. With an optimal amount of stabilization, SP concentration is high without stimuli, and SP readily converts to MC in the presence of force or UV light. Strong electron withdrawing groups at R_2 stabilize MC such SP concentration is low without stimuli which prevents triggered crosslinking. To achieve crosslinking via triggered 2:1 ion coordination in polymers requires tuning steric and electronic effects from the three R groups such that the following conditions are satisfied:

1. The equilibrium favors SP over MC in the absence of force or UV light.
2. With force or UV light, the equilibrium rapidly shifts favoring MC and reverts to SP removing stimuli.
3. When activated under stimuli, MC forms stable ion coordinations with a 2:1 ratio of molecules to ions.
4. Removing stimuli, rapidly shifts equilibrium back to SP removing the crosslinking ion coordinations and returning to the original state.

2.2 Tertiary Amine Spiropyran Polymer Synthesis

Initially, the project focused on using SP molecules with structures similar to those commercially available. We assessed the SP-ion coordination behavior by finding good metal ion candidates then constructing a Job plot. Good candidates for metal ions are divalent or higher to facilitate coordinating with multiple anionic ligands, and they significantly shift the UV-Vis absorbance spectrum. A significant spectrum shift produces different color solutions compared to a MC solution without metal ions. Having found a good ion candidate, we constructed a Job plot by measuring the UV-Vis absorbance maximum of the shifted spectrum at different concentration ratios of SP to ion. The location of the Job plot maximum determines the coordination ratio where a value of 0.5 [SP] / [SP + ion] corresopnds to a 1:1 ratio. With a nitro electron withdrawing group (R_2) and a methoxy coordinating sidechain (R_3), the commercially similar SP sample showed 1:1 ion coordination according to Job pot analysis (Figure 7).

The 1:1 coordination ratio from the Job plot lead us toward synthesizeing tertiary amine coordinating sidechains based on examples in literature. Following Scheme 4, the 1-(2-hydroxyethyl)-2,3,3-trimethyl-3H-indol-1-ium iodide component was synthesized in two steps from the condensation (**2**) of phenylhydrazine hydrochloride and 3-methlybutan-2-one and subsiquent S_N2 displacement (**3**) of 2-iodoethanol. The synthesis of the *o*-hydroxybenzaldehyde component was in one step via the S_N2 displacement (**4**) of 3-(chloromethyl)-2-hydroxy-5-nitrobenzaldehyde with 4-hydroxypiperidine. In situ

generation of the 2-methyleneindoline via deprotonation then condensation of the two SP components produced a *tert*-amine SP (**5**) that was copolymerized into a polyurethane (**6**). The resulting polymer maintained a red color in solid state and solution and showed no ion coordinating character. Based on the constant red color in the absence of force or UV light stimuli, the chemical environment in solid state and solution favors MC. Since this did not satisfy condition 1 for triggered ionic crosslinking, a different set of R groups must be used. The strongly electron with drawing character of the nitro group (R_2) may be too stabilizing which causes a higher MC concentration compared to SP.

If the electron with drawing power of a nitro group at R_2 is too strong, then a less powerful electron withdrawing group favors SP in the absence of stimuli to allow triggered ion coordination. Starting with the R_2 group preinstalled allows a greater variety of electron withdrawing groups in the *o*-hydroxybenzaldehyde synthesis. Drawing from the variety of *para*-substituted phenols, the Duff reaction (**7 & 8**) accesses *o*-hydroxybenzaledhydes with an additional aldehyde for the coordinating sidechain (Scheme 5).[17] I refined the reaction conditions to synthesize dialdehyde products in good yield from two *para*-substituted phenols with no monoaldehyde product observed by NMR. Efforts to selectively add a coordinating sidechain to one aldehyde are currently in progress. Possible pathways include reaction with secondary amine and alcohol containing moieties via reductive amination or imine condensation. Preventing a reaction with the second aldehyde has proven challenging.

2.3 Spirooxazine Synthesis

Similar to spiropyran, spirooxazines respond to UV light to favor a zwitterionic MC form that coordinates to ions as a ligand.[18] The main structural difference between spirooxazine and SP is a nitrogen in the spiro-ring which comes from replacing the aldehyde with a nitroso group in the synthesis (Scheme 6). Also, most spirooxazine examples in literature contain naphthalene as the R_2 group.[18] Using a less electron withdrawing group at R_2 and a coordinating sidechain heterocycle at R_3 may promote triggered 2:1 ion coordination.

Spirooxazine synthesis is the condensation of a 2-methlyeneindoline and an often naphthalene-based *o*-hydroxynitroso moiety (Scheme 6). The synthesis begins with the heterocycle formation (**9**) of 3-hydroxy-2-naphthohydrazide and carbon disulfide to form a 1,3,4-oxadiazole (Scheme 7). The sulfur adjacent to the oxadiazole undergoes ring opening (**10**) with propylene oxide to attach a polymerizable alcohol group. Elecrophoilic aromatic substitution (**11**) introduces an *o*-nitroso group on the naphthalene. After in situ generation of the 2-methyleneindoline, condensation (**12**) of the two spirooxazine components produces a naphthalene-based 1,3,4-oxadiazole-spirooxazine monomer.

The synthesized 1,3,4-oxadiazol-spirooxazine (**12**) showed photochromism in UV light at -70 °C but lost this property on warming to room temperature (Figure 8). This suggests that the naphthalene R_2 group does not adequately stabilize merocyanine until low temperatures. To promote room temperature photochromism, adding an electron donating methoxy as the $R_{1'}$ group stabilizes the positive charge that builds on the indoline-nitrogen in zwitterionic MC.[19] Another solution is to add electron withdrawing groups on naphthalene to stabilize the MC phenolate anion. However, this requires either starting with an electron withdrawing preinstalled on the hydrazine or ring functionalization after the nitroso aromatic substitution. If starting the synthesis with a preinstalled electron withdrawing group, the naphthalene has less electron density which reduces the effectiveness of the nitroso substitution. If installing the electron withdrawing group after nitroso substitution, the naphthalene lacks a directing group which leads to a mix a products. As another solution, adding metal ions stabilizes MC enough that some room temperature photochromism occurs (Figure 9). Combining effects from metal ions and a stabilizing electron withdrawing/donating group has the potential to promote significant room temperature photochromism. Beyond modification, the next steps for this pathway are to find other heterocycle syntheses which allow more variability in the types of electron withdrawing groups on naphthalene. Additionally, synthesis of a benzene-based 1,3,4-oxadiazole-spirooxzaine is in progress.

2.4 Conclusion

From the progress my collaborators and I made on this new project, we are close to finding good candidates for 2:1 ion coordination in spiropyran and spirooxazine polymer. A good candidate hinges on finding the right mix of merocyanine stabilization and ion coordination strength from sidechains to allow triggered ionic crosslinking in solution and solid state systems. This project provides an interesting synthetic challenge that will soon find success as a self-strengthening system.

As shown in both chapters, there is the potential to achieve intrinsic self-healing properties based on dynamic ionic interactions. Through sequence control and systematic structure-activity relationship studies, we will achieve control over properties of synthetic polymer systems rivaling those of biological polymers. New sequence-specific experimental techniques pave the way for polymer synthesis on a large scale with absolute control over monomer placement in a sequence. Understanding how monomers interact with ions leads to new self- healing materials where material lifetimes exceed current limitations. Through a reversible self-strengthening mechanism, materials experience extended lifetimes capable of surviving repeated cycles of stress and relaxation. These self-healing materials that improve in response to their environment are fundamental to the future of materials.

2.5 Schemes and Figures

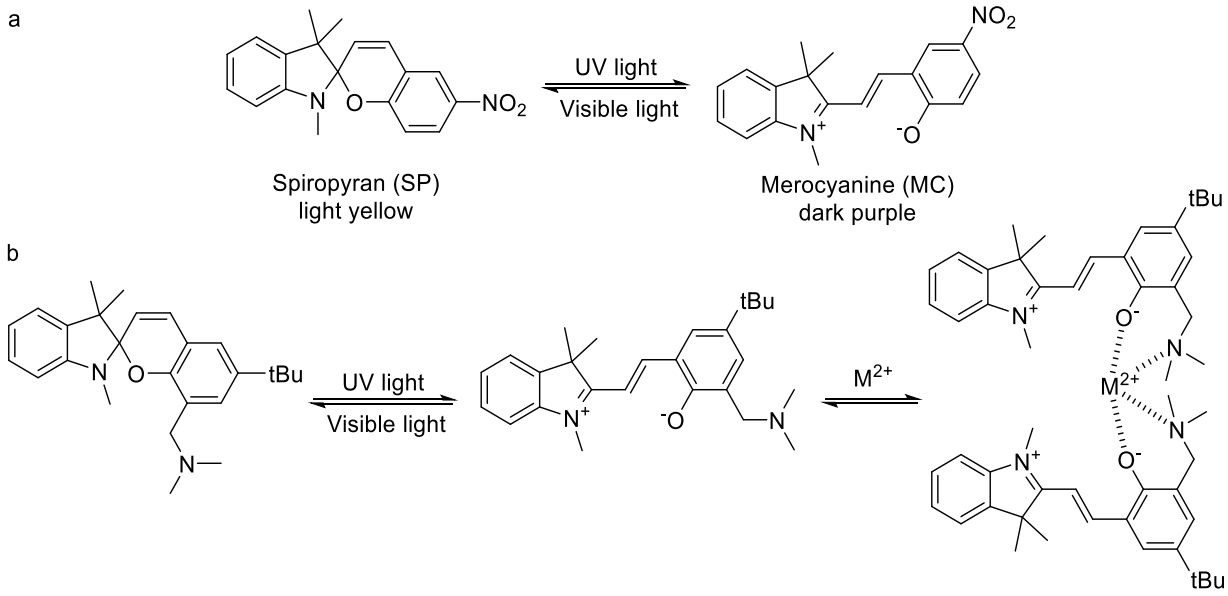

Scheme 1. The general spiropyran to merocyanine equilibrium (a). An example of spiropyran with a *tert*-amine sidechain coordinating to metal ions in a 2:1 ratio (b).[20]

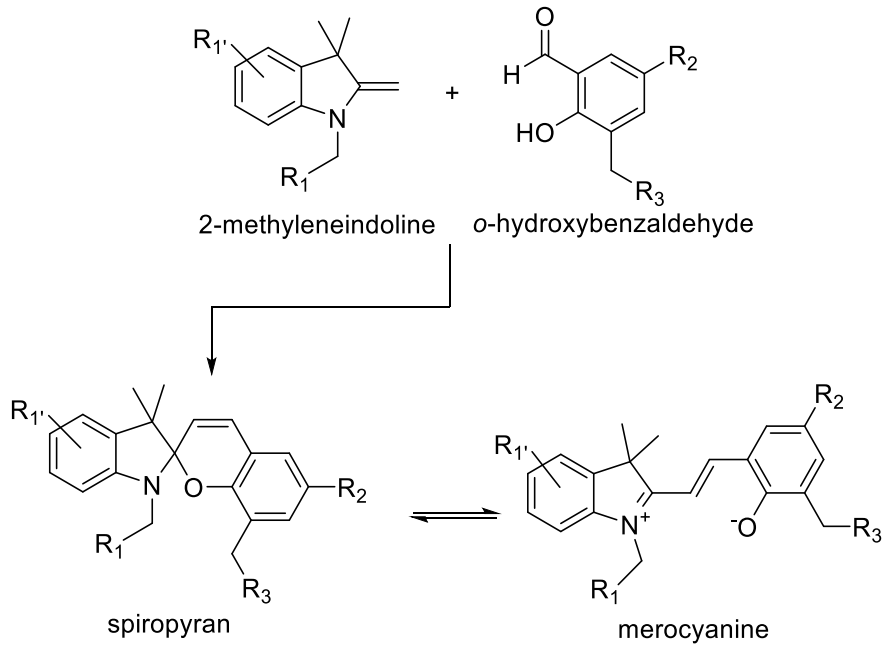

Scheme 2. General spiropyran synthesis is the condensation between a 2-methyleneindoline and an *o*-hydroxybenzaldehyde. The R groups show the sites for modification.

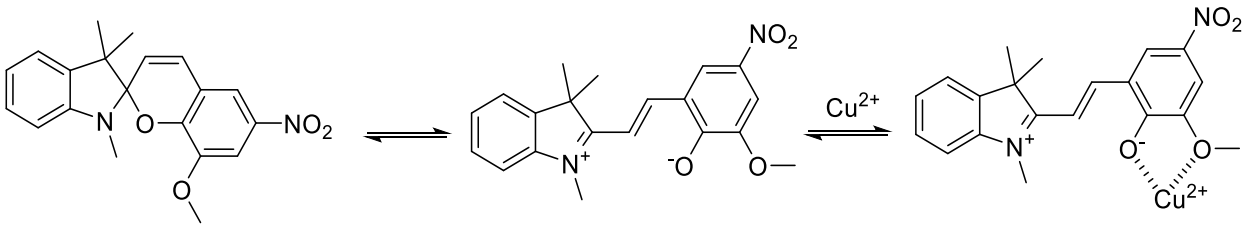

Scheme 3. SP-ion coordination for R_1 = methyl, R_2 = nitro, and R_3 = methoxy.

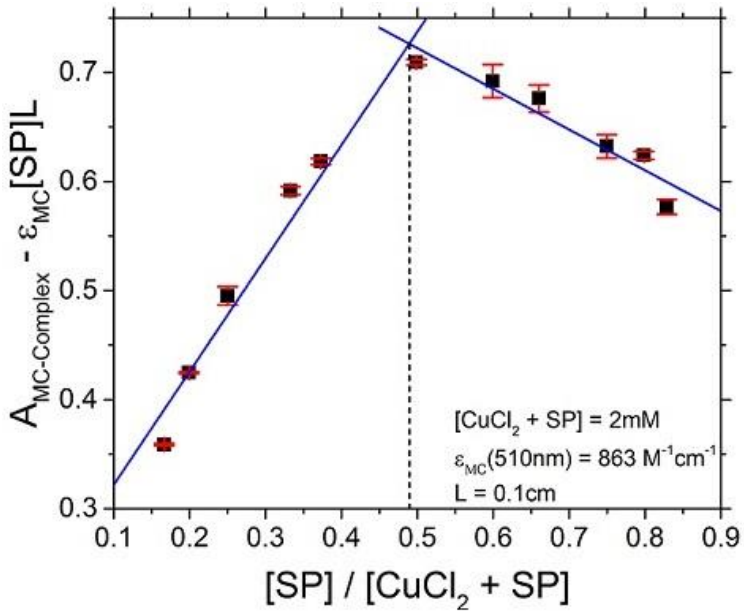

Figure 7. Job plot analysis for the SP-ion coordination of R_1 = methyl, R_2 = nitro, and R_3 = methoxy. The maximum at 0.5 [SP] / [$CuCl_2$ + SP] indicates 1:1 SP:ion coordination.

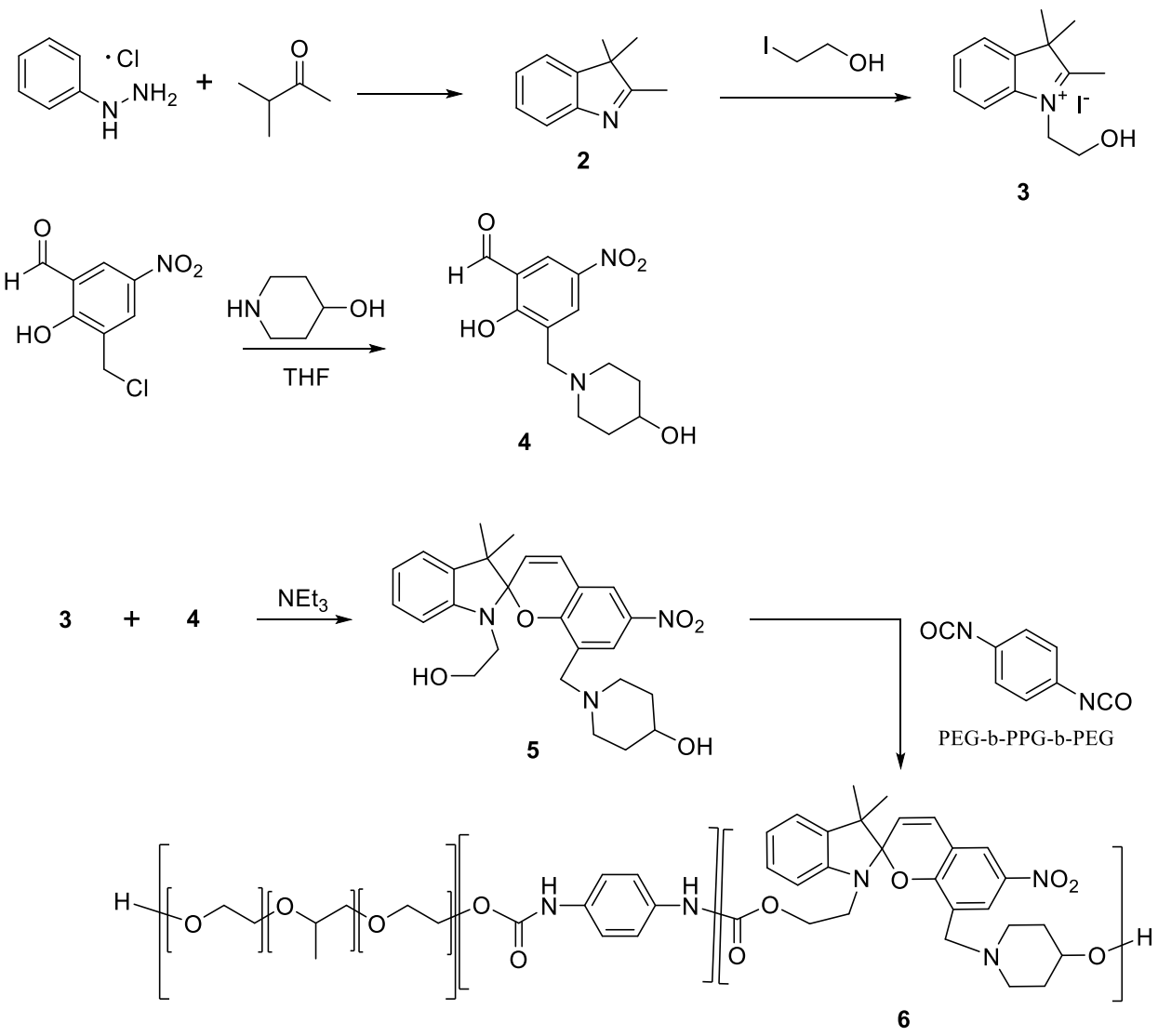

Scheme 4. The synthesis of a tertiary amine SP polymer.

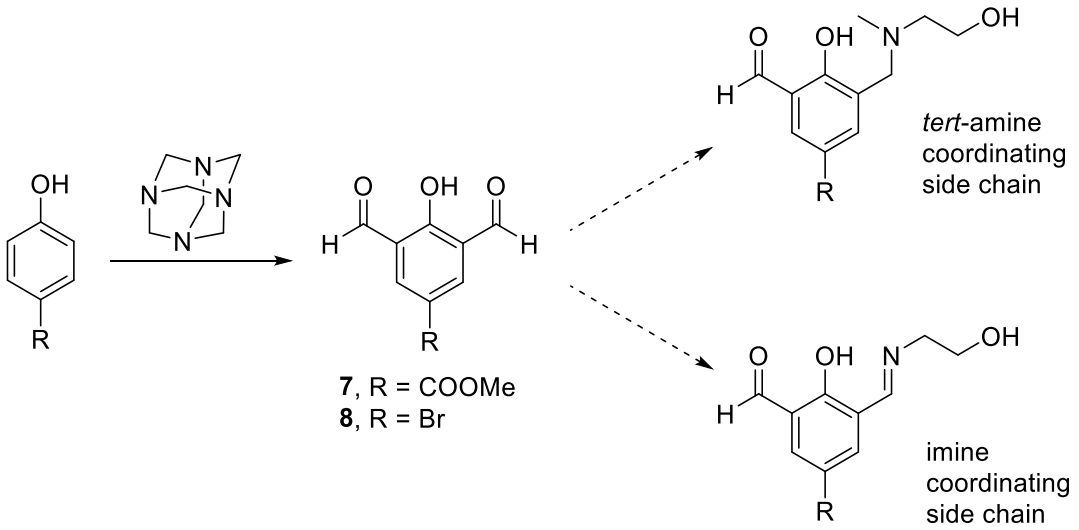

Scheme 5. Future directions for the *o*-hydroxybenzaldehyde synthesis via Duff reaction of a variety of *para*-substituted phenols.

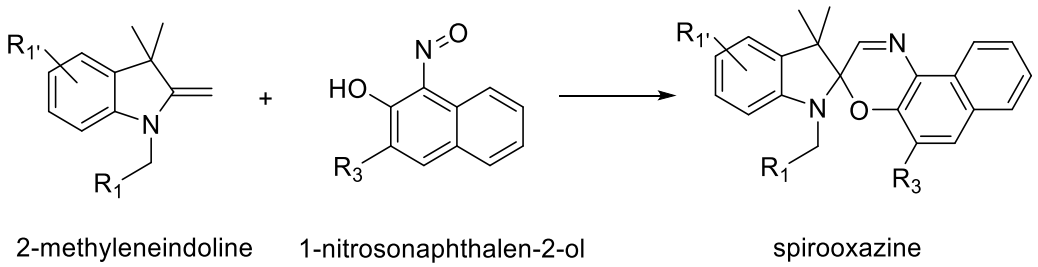

Scheme 6. General spirooxazine synthesis.

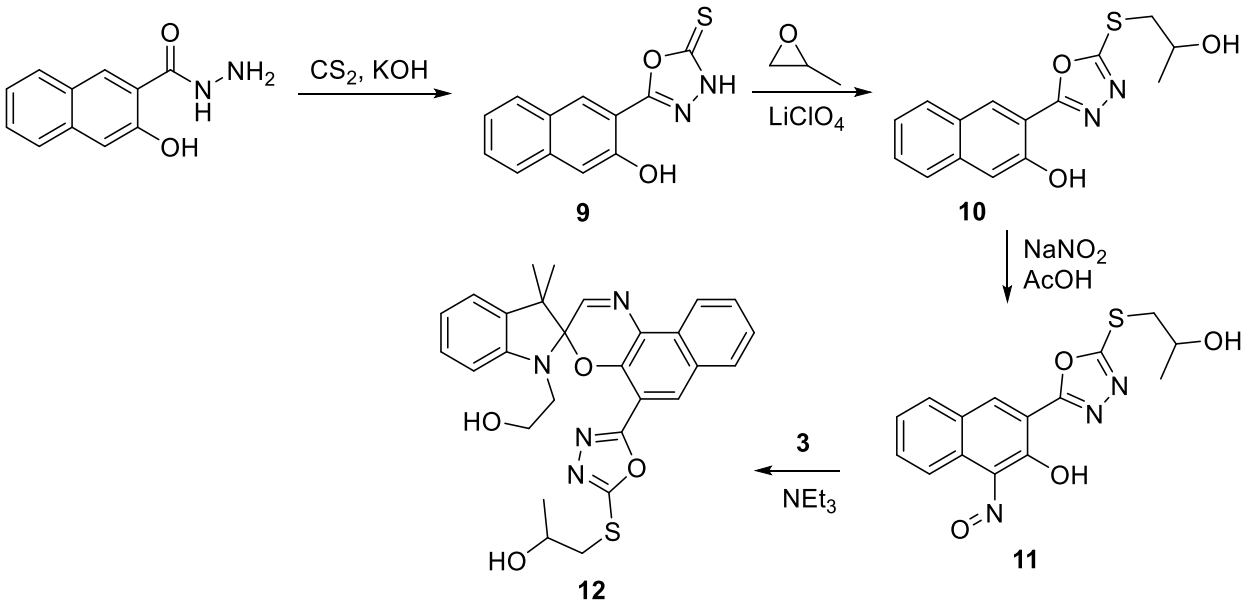

Scheme 7. The synthesis of a spirooxazine monomer.

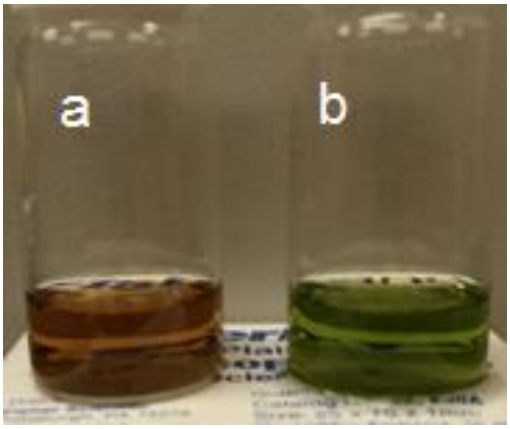

Figure 8. Solutions of the synthesized spirooxazine at -70 °C after irradiation with UV light (a) and without UV-light (b). The difference in color indicates photochromism.

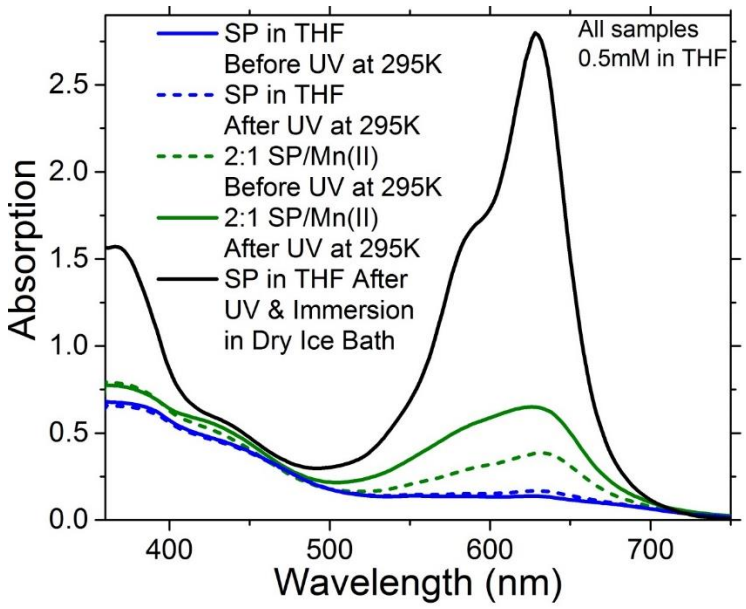

Figure 9. UV-Vis measurements for the synthesized spirooxazine (**12**) before and after UV light irradiation without metal ions (blue), with Mn^{2+} ions present (green), and after UV light at -70 °C. Metal ions promote some room temperature photochromism based on the difference between the solid and dotted green lines.

2.6 Experimental Information

All chemicals were purchased commercially from Sigma-Aldrich and used without purification unless otherwise noted. Ethanol was purchased from Decon Labs. Glacial acetic acid was from J.T. Baker. From Alfa Aesar, phenylhydrazine hydrochloride and 3-methylbutan-2-one were purchased. The 3-(chloromethyl)-2-hydroxy-5-nitrobenzaldehyde was from TCI Chemicals. From Acros Organics, 4-hydroxypiperidine was purchased. Carbon disulfide and potassium hydroxide were purchased from Fisher Scientific.

UV-Vis Analysis and Job Plot Construction

UV-Vis data were collected over a wavelength range of 360-700 nm. Samples were prepared using the method of continuous variations named Job's method. For all measured solutions, total concentration of [SP + metal ion] was held constant at 2 mM. The metal chloride was used in all samples. The Job plot was constructed by measuring the absorbance at peak wavelength for varying ratios of [SP] to [metal ion]. To eliminate any absorbance from non-coordinating SP, the absorbance from an SP sample without metal ion was subtracted. Absorbance from metal ions without SP was assumed to me minimal and was not subtracted.

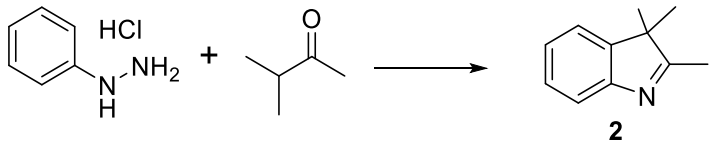

2

(2) 2,3,3-trimethyl-3H-indole:

To a 300 mL round bottom flask, phenylhydrazine hydrochloride (35 mmol) and ethanol (165 mL) were added. To the stirring solution, 3-methylbutan-2-one (35 mmol) was added. Solution was heated to reflux under N_2 atmosphere at 100 °C for 19 h. After cooling, red solution was concentrated *in vacuo*. Product was purified by silica gel column in 3:1 hexanes:ethyl acetate. 50% yield; 1H NMR (d_6-DMSO) δ: 7.43 (dd, J = 7.7, 1.1 Hz, 1H, ArH), 7.38 (dd, J = 7.5, 1.1 Hz, 1H, ArH), 7.25 (tt, J = 7.5, 1.1 Hz, 1H, ArH), 7.15 (tt, J = 7.4, 1.1 Hz, 1H, ArH), 2.19 (s, 3H, CH_3), 1.21 (s, 6H, CH_3); ^{13}C NMR (d_6-DMSO) δ: 188.2, 154.3, 146.6, 127.9, 125.4, 122.2, 119.9, 53.8, 23.2, 15.7, TLC (3:1 hexanes:ethyl acetate) R_f = 0.21

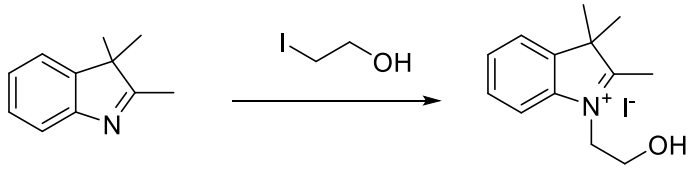

2 **3**

(3) 1-(2-hydroxyethyl)-2,3,3-trimethyl-3H-indol-1-ium iodide:

In a 200 mL round bottom flask, 2,3,3-trimethyl-3H-indole (**2**) (193 mmol) and 2-iodoethanol (244 mmol) were dissolved in anhydrous acetonitrile (70 mL). Solution was heated to reflux at 90 °C for 24 h. After cooling to room temperature, product was precipitated with diethyl ether. The light yellow solid product was filtered and washed with diethyl ether, toluene, and hexanes. 92% yield; ^{1}H NMR (d_6-DMSO) δ: 7.97 (m, 1H, ArH), 7.85 (m, 1H, ArH), 7.62 (m, 2H, ArH), 4.60 (t, J = 5.0 Hz, 2H, CH_2N^+), 3.88 (t, J = 4.9 Hz, 2H, CH_2OH), 2.83 (s, 3H, CH_3), 1.55 (s, 6H, CH_3); ^{13}C NMR (d_6-DMSO) δ: 197.7, 141.8, 141.1, 129.3, 128.8, 123.4, 115.5, 57.8, 54.2, 50.3, 22.0, 14.4

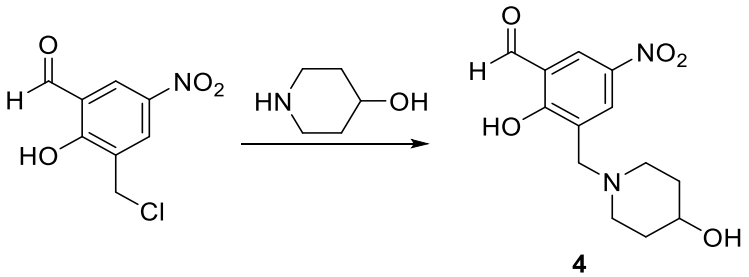

4

(4) 2-hydroxy-3-((4-hydroxypiperidin-1-yl)methyl)-5-nitrobenzaldehyde:

In a 100 mL round bottom flask, 4-hydroxypiperidine (118 mmol) was dissolved in anhydrous THF (30 mL). Solution was heated to 62 °C under N_2 atmosphere. A separate solution of 3-(chloromethyl)-2-hydroxy-5-nitrobenzaldehyde (24 mmol) in 20 mL anhydrous THF was added to the 4-hydroxypiperidine solution via syringe pump at 12 µL/min. After 32 h, addition was complete and solution was stirred for an additional 8 h at 62 °C under N_2 atmosphere. After cooling to room temperature, reaction mixture was concentrated *in vacuo*, and product was precipitated with water. Product was filtered, washed with water, and lyophilized. 94% yield; ^{1}H NMR (d_6-DMSO) δ: 10.17 (s, 1H, CHO), 8.27 (d, J = 3.2 Hz, 1H, ArH), 8.16 (d, J = 3.3 Hz, 1H, ArH), 4.99 (br s, 1H, OH), 4.13 (s, 2H, $ArCH_2N$), 3.78 (m, 1H, C**H**OH), 3.25 (m, 2H, CH_2), 3.07 (m, 2H, CH_2), 1.92 (m, 2H, CH_2), 1.67 (m, 2H, CH_2); ^{13}C NMR (d_6-DMSO) δ: 190.9, 179.2, 132.4, 130.2, 127.6, 124.4, 123.3, 56.0, 41.4, 31.2, 30.9; MS (HRESI): (M-H) m/z = 279.0975, calc. 279.0981 $C_{13}H_{15}N_2O_5$

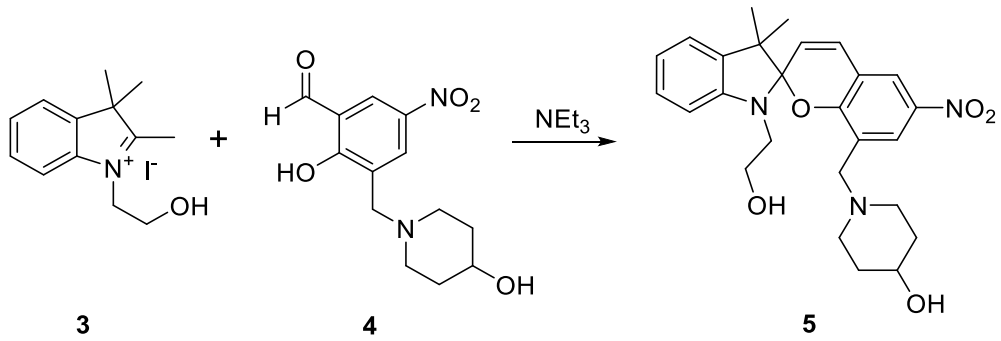

3 **4** **5**

(5) 1-((1'-(2-hydroxyethyl)-3',3'-dimethyl-6-nitrospiro[chromene-2,2'-indolin]-8-yl)methyl)piperidin-4-ol:

To a 300 mL round bottom flask, 1-(2-hydroxyethyl)-2,3,3-trimethyl-3H-indol-1-ium iodide (**3**) (15.9 mmol) and 2-hydroxy-3-((4-hydroxypiperidin-1-yl)methyl)-5-nitrobenzaldehyde (**4**) (15.9 mmol) were added. Solids were dissolved in ethanol (100 mL), and triethylamine (47.7 mmol) was added to reaction mixture. Solution was heated to reflux at 100 °C under N_2 atmosphere for 6.5 h. After cooling, reaction mixture was concentrated *in vacuo* to promote precipitation. After allowing reaction mixture to rest overnight, precipitate was filtered and dried *in vacuo*. 65% yield; MS (HRESI): (M+H) m/z = 466.2346, calc. 466.2342 $C_{26}H_{32}N_3O_5$

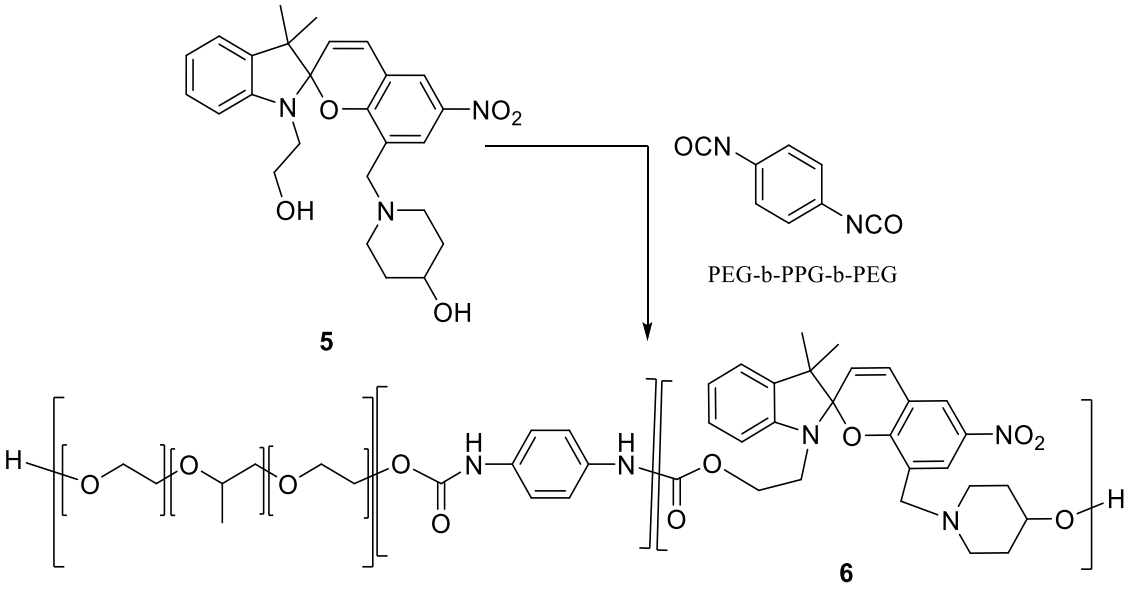

(6) Polyurethane Spiropyran Copolymer Synthesis:

The polyethylene glycol-b-polypropylene glycol-b-polyethylene glycol chain extender and spiropyran (**5**) were dissolved in anhydrous DMF. Solution was stirred for 10 min under N_2 atmosphere. Phenylenediisocyanate was added to solution with maintain a 1:1 ration of isocyanate to hydroxide groups. Triethanolamine (1-10 mol%) crosslinker was added to solution. Mixture was stirred for 5 min at room temperature and quickly transferred to Delrin dogbone-shaped molds. Mixture was polymerized in the molds at 70 °C under N_2 atmosphere for 48 h to produce a red elastic polymer.

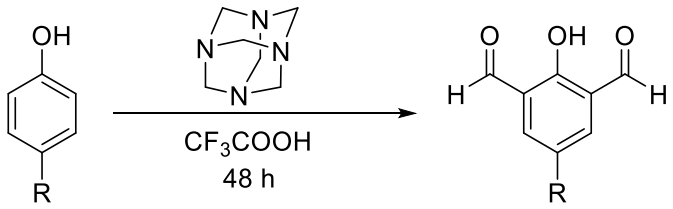

(7) Methyl 3,5-diformyl-4-hydroxybenzoate:

A 500 mL round bottom flask was charged with methyl 4-hydroxybenzoate (69 mmol) and hexamethylenetetramine (550 mmol). Solid mixture was dissolved in trifluoroacetic acid (172 mL) and heated to reflux at 110 °C. After 48 h, reaction mixture was allowed to cool to room temperature. Reaction was quenched with 4 M $HCl_{(aq)}$ (350 mL) and stirred in ice bath for 30 min. Yellow-orange suspension was filtered and washed with cold water. Precipitate crystals were formed in the filtrate at the interface between water washings and reaction mixture on standing overnight. Precipitate was filtered and collected as pure product without further purification. Additional precipitation was induced by adding a

layer of water to filtrate. 78% yield; ^{1}H NMR ($CDCl_3$) δ: 11.99 (br s, 1H, OH), 10.20 (s, 2H, CHO), 8.56 (s, 2H, ArH), 3.89 (s, 3H, OMe); ^{13}C NMR ($CDCl_3$) δ: 192.0, 166.5, 164.9, 139.0, 123.2, 122.8, 52.8; MS (ESI): m/z = 208.0, calc. 208.0

(8) 5-bromo-2-hydroxy-isophthalaldehyde:

Procedure was the same as (**7**) except 4-bromophenol was substituted in the place of methyl 4-hydroxybenzoate. 73% yield; ^{1}H NMR (d_6-DMSO) δ: 11.61 (br s, 1H, OH), 10.19 (s, 2H, CHO), 8.11 (s, 2H, ArH); ^{13}C NMR (d_6-DMSO) δ: 191.6, 161.5, 139.2, 126.4, 112.0; MS (HRESI): m/z=227.9429, calc. 227.9422 $C_8H_5O_3Br$

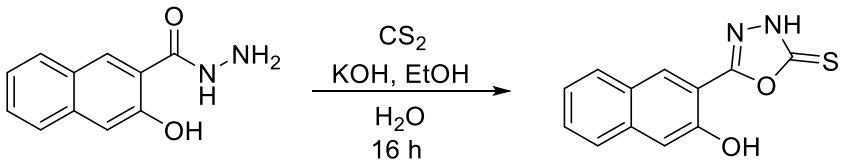

9

(9) 5-(3-hydroxynaphthalen-2-yl)-1,3,4-oxadiazole-2(3H)-thione:

To a 1 L round bottom flask, 3-hydroxy-2-naphthohydrazide (50 mmol) and ethanol (50 mmol) were added. While stirring, 2M $KOH_{(aq)}$ (25 mL) was added. To the stirring yellow suspension, CS_2 (50 mmol) was added. Reaction mixture was heated to reflux at 95 °C. A yellow foam and H_2S were produced during the reaction. After refluxing overnight, H_2S production ceased, and a yellow suspension remained. Reaction mixture was poured into cold water (125 mL). Suspension was made acidic with 1M $HCl_{(aq)}$ resulting in white suspension. White solid was filtered and dried *in vacuo*. Product was recrystallized from hot ethanol to produce a fluffy off-white solid. 60% yield; ^{1}H NMR (d_6-DMSO) δ: 10.5 (br s, 1H, ArNH), 8.3 (s, 1H, ArH), 7.92 (d, J = 8.2 Hz, 1H, ArH), 7.73 (d, J = 8.3 Hz, 1H, ArH), 7.48 (t, J = 7.5 Hz, 1H, ArH), 7.36 (s, 1H, ArH), 7.32 (t, J = 7.5 Hz, 1H, ArH); ^{13}C NMR (d_6-DMSO) δ: 177.9 (S=C), 160.2, 153.3, 136.4, 131.1, 129.3, 129.1, 127.5, 126.5, 124.6, 112.8, 111.3; MS (HRESI): m/z=245.0380, calc. 245.0385 $C_{12}H_9N_2O_2S$

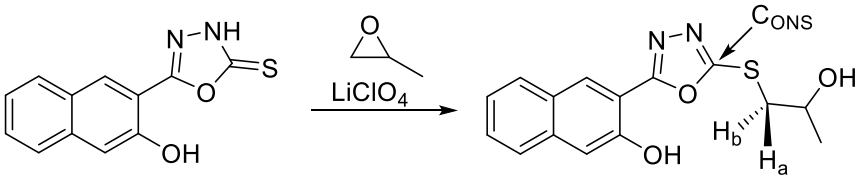

9 **10**

(10) 3-(5-((2-hydroxypropyl)thio)-1,3,4-oxadiazol-2-yl)naphthalen-2-ol:

To a 50 mL round bottom flask, 5-(3-hydroxynaphthalen-2-yl)-1,3,4-oxadiazole-2(3H)-thione (**9**) (13.9 mmol) and $LiClO_4$ (27.8 mmol) were added. Solids were dissolved in anhydrous acetonitrile (6 mL) and anhydrous dimethlformamide (12 mL). Solution was stirred for 15 min under positive N_2 pressure. Propylene oxide (14.2 mmol) was added, and reaction mixture was stirred at room temperature for 16 h. Product was precipitate by slow addition of water. Precipitated solid was filtered and washed with water and hexanes. Product was dried by lyophilization. 74% yield; ^{1}H NMR (d_6-DMSO) δ: 10.35 (br s, 1H, ArOH), 8.42 (s, 1H, ArH), 7.96 (d, J = 8.3 Hz, 1H, ArH), 7.77 (d, J = 8.3 Hz, 1H, ArH), 7.51 (ddd, J = 8.2, 6.7, 1.2 Hz, 1H, ArH), 7.40 (s, 1H, ArH), 7.36 (ddd, J = 8.1, 6.7, 1.2 Hz, 1H, ArH), 4.03 (td, J = 7.2, 6.8 Hz, 1H, C**H**OH), 3.43 (dd, J = 13.0, 4.8 Hz, 1H, H_a/H_b), 3.33 (dd, J = 13.0, 6.9 Hz, 1H, H_a/H_b), 1.22 (d, J = 6.2 Hz, 3H, CH_3); ^{13}C NMR (d_6-DMSO) δ: 165.0 (C_{ONS}), 164.9, 153.1, 136.4, 130.8, 129.2, 129.1, 127.7, 126.7, 124.7, 113.0, 111.4, 65.5, 41.4, 23.1; 2D-NMR HMBC (d_6-DMSO): 3-bond connection between C_{ONS} and H_a/H_b; MS (HRESI): m/z=303.0806, calc. 303.0800 $C_{15}H_{15}N_2O_3S$

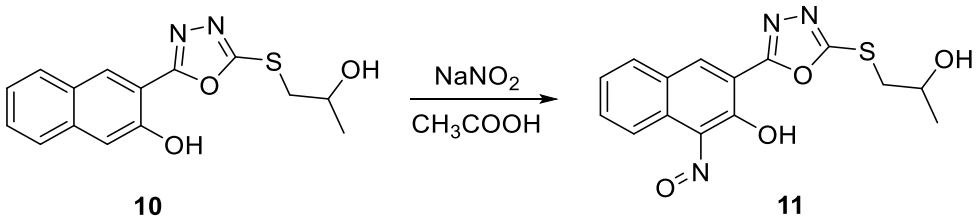

10 **11**

(11) 3-(5-((2-hydroxypropyl)thio)-1,3,4-oxadiazol-2-yl)-1-nitrosonaphthalen-2-ol:

To a 100 mL round bottom flask, 3-(5-((2-hydroxypropyl)thio)-1,3,4-oxadiazol-2-yl)naphthalen-2-ol (**10**) (28.8 mmol) was added and dispersed in acetic acid at room temperature. To lower the freezing point, water (20 mL) was added, and solution was cooled in ice bath. A solution of $NaNO_2$ (86.4 mmol) in water (27 mL) was added dropwise to reaction mixture over 28 min. After addition was complete, solution was stirred in ice bath for 2.5 h. Product was precipitated by slow addition of cold water and filtered. Product was washed with cold water and dried by lyophilization over 2 days. 82% yield; ^{1}H NMR (d_6-Acetone) δ: 8.48 (s, 1H, ArH), 7.88 (dd, J = 7.6, 1.6 Hz, 1H, ArH), 7.68 (td, J = 7.8, 1.6 Hz, 1H, ArH), 7.62 (td, J = 7.5, 1.4 Hz, 1H, ArH), 5.05 (br s, 1H, OH), 4.07 (m, 1H, C**H**OH), 3.44 (dd, J = 13.0, 4.8 Hz, 1H, SCH_2), 3.34 (dd, J = 13.0, 7.0 Hz, 1H, SCH_2), 1.25 (d, J = 6.2 Hz, 3H, CH_3); MS (HRESI): (M+H) m/z = 332.0698, calc. 332.0705 $C_{15}H_{14}N_3O_4S$

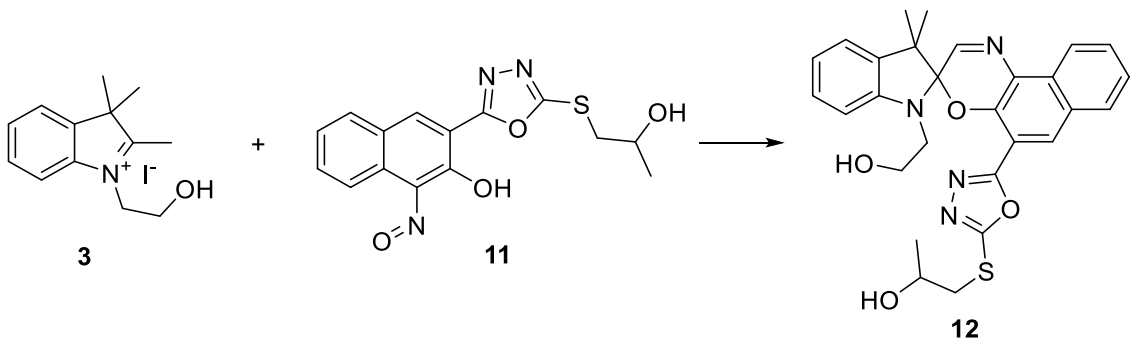

(12) 1-((5-(1-(2-hydroxyethyl)-3,3-dimethylspiro[indoline-2,3'-naphtho[2,1-b][1,4]oxazin]-5'-yl)-1,3,4-oxadiazol-2-yl)thio)propan-2-ol:

To a 5 mL round bottom flask, 3-(5-((2-hydroxypropyl)thio)-1,3,4-oxadiazol-2-yl)-1-nitrosonaphthalen-2-ol (**11**) (1.2 mmol) and 1-(2-hydroxyethyl)-2,3,3-trimethyl-3H-indol-1-ium iodide (**3**) were added and dissolved in anisole (2 mL). Triethlyamine (2.4 mmol) was added to the solution. Reaction mixture was heated to 65 °C for 4 h and slowly cooled to room temperature. Mixture was stirred at room temperature for 16 h. Reaction mixture was concentrated *in vacuo*, and water was added to induce precipitation. Aceton was added to dissolve precipitate, and product was precipitated with hexanes. Product was filtered and dried via lyophilization. 7% yield; MS (HRESI): (M+H) m/z = 517.1910, calc. 517.1910 $C_{28}H_{29}N_4O_4S$

2.7 References

14. Craig, S. L. et al. *Nat. Chem.*, **2013**, *5*, 757-761.
15. Kloxin, C. J. et al. *Adv. Mater.*, **2015**, *27*, 8007-8010.
16. Klajn, R. *Chem. Soc. Rev.*, **2014**, *43*, 148-184.
17. Svenstrup, N. et al. *Synthesis*, **1998**, 1029-1032.
18. Fedorova, O. A. et al. *J. Photochem. Photobiol. C*, **2011**, *12*, 209-236.
19. Metelitsa, A. V. et al. *Int. J. Photoenergy*, **2004**, *06*, 199-204.
20. Micheau, J. C. et al. *Russ. Chem. Bull, Int. Ed.*, **2009**, *58*, 1329-1337.